

DETECTION OF HC₅N AND HC₇N ISOTOPOLOGUES IN TMC-1 WITH THE GREEN BANK TELESCOPE

ANDREW M. BURKHARDT,¹ ERIC HERBST,^{2,1} SERGEI KALENSKII,³ MICHAEL C. MCCARTHY,⁴ ANTHONY J. REMIJAN,⁵ AND
BRETT A. MCGUIRE^{5,4,*}

¹*Department of Astronomy, University of Virginia, Charlottesville, VA 22903, USA*

²*Department of Chemistry, University of Virginia, Charlottesville, VA 22903, USA*

³*Astro Space Center, Lebedev Physical Institute, Russian Academy of Sciences, Moscow, Russia*

⁴*Harvard-Smithsonian Center for Astrophysics, Cambridge, MA 02138, USA*

⁵*National Radio Astronomy Observatory, Charlottesville, VA 22903, USA*

ABSTRACT

We report the first interstellar detection of DC₇N and six ¹³C-bearing isotopologues of HC₇N toward the dark cloud TMC-1 through observations with the Green Bank Telescope, and confirm the recent detection of HC₅¹⁵N. For the average of the ¹³C isotopomers, DC₇N, and HC₅¹⁵N, we derive column densities of $1.9(2)\times 10^{11}$, $2.5(9)\times 10^{11}$, and $1.5(4)\times 10^{11}$ cm⁻², respectively. The resulting isotopic ratios are consistent with previous values derived from similar species in the source, and we discuss the implications for the formation chemistry of the observed cyanopolyynes. Within our uncertainties, no significant ¹³C isotopomer variation is found for HC₇N, limiting the significance CN could have in its production. The results further show that, for all observed isotopes, HC₅N may be isotopically depleted relative to HC₃N and HC₇N, suggesting that reactions starting from smaller cyanopolyynes may not be efficient to form HC_nN. This leads to the conclusion that the dominant production route may be the reaction between hydrocarbon ions and nitrogen atoms.

arXiv:1711.07495v2 [astro-ph.GA] 22 Nov 2017

Corresponding author: Andrew M. Burkhardt & Brett A. McGuire
amb3au@virginia.edu & bmcguire@nrao.edu

* B.A.M. is a Hubble Fellow of the National Radio Astronomy Observatory

1. INTRODUCTION

Carbon-chain molecules are a critically important family within the interstellar medium (ISM); they represent $\sim 40\%$ of all detected species and play a major role in the formation of more complex chemistry. Carbon chains with interstellar detections include: carbenes (McCarthy et al. 1997), polyynes (Irvine et al. 1981; Bell et al. 1997; Snyder et al. 2006; Remijan et al. 2006), unsaturated hydrocarbons (Cernicharo et al. 2001), and the newly detected HC_nO family (McGuire et al. 2017). Furthermore, it has been suggested that they may be important precursors to the formation of polycyclic aromatic hydrocarbons (PAHs) (Guzman-Ramirez et al. 2011), which are likely to be routine targets of observation when the James Webb Space Telescope is launched in 2019 (Kirkpatrick et al. 2017).

Reactions of unsaturated carbon-chain molecules (i.e. species whose available carbon valence electrons are not all bonded to atoms so that the chain contains more double and triple carbon-carbon bonds) are often efficient in the ISM, but have many product channels for which branching ratios are not known. Because of the lack of available laboratory measurements of the dominant reaction mechanisms and rate coefficients for these branching fractions, the ability to directly investigate these pathways through interstellar observations is therefore appealing. One way to probe the underlying chemistry is through the study of the isotopologues (molecules that differ only in isotopic composition (e.g. HCCCN vs H^{13}CCCN) and isotopomers (molecules that contain the same isotopic composition, but differ in the isotope positions (e.g. H^{13}CCCN vs HCC^{13}CN)) of a species. For many molecules, specific relative isotopic fractions or isotopomer configurations can possibly constrain the dominant production method or precursors.

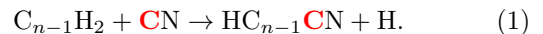
TMC-1, one of the prototypical dark cloud cold cores, has been the subject of intense astrochemical study. Observationally, it has been the source of many new molecular detections, including a large fraction of the known unsaturated carbon-chains (Kaifu et al. 2004; Snyder et al. 2006; McCarthy et al. 2006; Remijan et al. 2006; McGuire et al. 2017). Furthermore, TMC-1 is dynamically stable, characterized by narrow line widths ($\sim 0.3 \text{ km s}^{-1}$), cold excitation temperatures (5-10 K), and a low line density (~ 1 line per 200 km s^{-1} for reasonable integration times with the GBT), making it ideal for the unambiguous detection of new molecules. Finally, because of its simple physical history, it is an ideal source to test chemical network models (Hasegawa et al. 1992; Herbst & Millar 2008; Ruaud et al. 2016; Majumdar et al. 2017).

Cyanopolyynes, a family of linear molecules of the form HC_nN (where $n = 3, 5, 7, \text{ etc.}$, henceforth) with alternating single and triple-bonded carbon atoms, have been detected in cold dark clouds (Brotten et al. 1978), the expanding envelopes of evolved stars (Bell et al. 1992), and even external galaxies (Mauersberger et al. 1990). It has been shown that, unlike many carbon-chains, the $^{12}\text{C}/^{13}\text{C}$ ratio for HC_5N is constant even into subsequent stages of star formation through observations of warm carbon-chain chemistry in the low-mass star-forming region L1527 (Araki et al. 2016; Taniguchi et al. 2016b). This finding implies that the formation of cyanopolyynes may occur primarily under dark cloud conditions. These species then remain as relics in subsequent stages of star formation, and have a unique underlying chemistry compared with other carbon-chain molecules. However, recent observations of a more evolved core, L134N, suggest that other formation pathways may dominate at later times (Taniguchi et al. 2017).

Of particular interest, Loomis et al. (2016) recently discussed the non-detection of HC_{11}N , which deviates from the log-linear abundance vs molecular size trend seen for smaller cyanopolyynes (Bujarrabal et al. 1981; Bell et al. 1997; Ohishi & Kaifu 1998; Remijan et al. 2006). Although this trend was previously thought to arise from a consistent set of gas-phase reactions that add carbons directly to smaller HC_nN species (Remijan et al. 2005; Winnewisser & Walmsley 1979; Bujarrabal et al. 1981; Fukuzawa et al. 1998), it was proposed by Loomis et al. (2016) that cyclisation processes may need to be considered to accurately explain this deviation. It is clear, therefore, that the chemistry of this family of species is not fully understood, especially at larger molecular sizes, and further study is needed.

For the cyanopolyne family, Takano et al. (1998) and Taniguchi et al. (2016a) discussed the potential prominence of three formation routes, among others, for a given molecule (HC_nN), which could each result in different $^{12}\text{C}/^{13}\text{C}$ fractionations. Each of these numbered mechanisms is discussed below, and, for clarity, sources of carbon atoms which could result in ^{13}C fractionation are traced from reactants to products in example reactions in red.

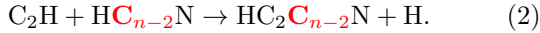
Mechanism 1 - The reaction between hydrocarbon molecules and the CN radical, including



Here, the difference between the isotopic fractions of the CN carbon atom and the carbene C_{n-1}H_2 carbon

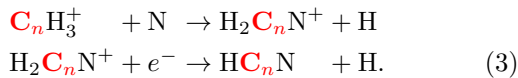
atoms results in asymmetric fractionation along the chain (Herbst & Leung 1990; Fukuzawa et al. 1998).

Mechanism 2 - Reactions of the next-smallest cyanopolyynes (e.g. HC_5N vs HC_3N) with hydrocarbons, such as



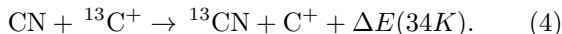
For this case, many of the isotopomers would have similar $^{12}\text{C}/^{13}\text{C}$ ratios to their corresponding isotopomer of the precursor cyanopolyne, with potentially some small variations depending on the precursor hydrocarbon (Schiff & Bohme 1979; Huntress 1977).

Mechanism 3 - Reactions of nitrogen atoms and hydrocarbon ions containing the same number of carbon atoms. One such example is



In this scenario, $^{12}\text{C}/^{13}\text{C}$ fractionation would be set by this precursor ion. Assuming the ion’s carbon atoms are sufficiently scrambled, this manifests as no significant variations among the isotopomers’ ratios (Herbst 1983; Herbst et al. 1984; Knight et al. 1986).

Previously, the $^{12}\text{C}/^{13}\text{C}$ fractionation had only been studied for cyanoacetylene (HC_3N) and cyanodiacetylene (HC_5N). For HC_3N , Takano et al. (1998) found that toward TMC-1 there was a $\sim 40\%$ abundance enhancement of the isotopomer with the ^{13}C residing next to the nitrogen atom ($\text{HC}_2^{13}\text{CN}$) relative to the other two species, suggesting that the primary formation route could be the neutral reactions between the abundant CN and C_2H_2 (Mechanism 1). This enhancement in the ^{13}C is thought to result from the exothermic exchange reaction given by



Because the reaction is exothermic, only the forward process is efficient at the cold temperatures within dark clouds, which results in an enhanced ^{13}C fractionation in CN compared with the carbene precursors whose exchange reactions are much less efficient (Benson & Myers 1989; Watson et al. 1976). This enhancement of ^{13}C in CN relative to measured solar system isotopic fractions has been ubiquitously observed in Galactic molecular clouds (Milam et al. 2005).

Meanwhile, Taniguchi et al. (2016a) found that there was no significant difference in the abundance of the ^{13}C -isotopomers of HC_5N toward TMC-1, suggesting that the primary formation route for HC_5N could be from reactions of N with hydrocarbon ions (such as C_5H_3^+ , C_5H_4^+ , and C_5H_5^+).

It is also important to compare these results to the dominant formation routes within chemical network models. Significant work has been done for this molecular family by Loomis et al. (2016) and McGuire et al. (2017) who adapted the KIDA network within NAUTILUS (Ruaud et al. 2016). At the model’s time of best agreement, multiple formation routes significantly contributed ($>30\%$) to the formation of cyanopolyynes, many of which do not necessarily agree with the observational constraints.

We have recently performed deep observations of TMC-1, which has resulted in the interstellar detection of several new molecules (McGuire et al. 2017). Here, we present the detection of six of the seven possible ^{13}C -bearing isotopomers of HC_7N , as well as DC_7N . In addition, we confirm the recent detection of HC_5^{15}N . The observations are presented in §2, a review of the laboratory spectroscopy is given in §3, the results and analysis are discussed in §4, and a discussion of the astrochemical implications is given in §5.

2. OBSERVATIONS

Observations, described previously by McGuire et al. (2017), toward TMC-1 were performed on the 100 m Robert C. Byrd Green Bank Telescope (GBT) in Green Bank, WV with the K-band Focal Plane Array (KFPA) along with the Versatile GBT Astronomical Spectrometer (VEGAS) spectrometer backend. The beam size varied from 32-40'' across the observed frequency range, with a beam efficiency of ~ 0.92 . The VEGAS backend was configured for 187.5 MHz bandwidth and 1.4 kHz (0.02 km s^{-1}) spectral resolution. In two separate frequency setups, a total of ten individual passbands were observed for a total of 1875 MHz of spectral coverage between 18 and 24 GHz. The observations were centred on $\alpha(\text{J2000}) = 04^{\text{h}}41^{\text{m}}42^{\text{s}}.5$, $\delta(\text{J2000}) = 25^{\circ}41'27''.0$, with pointing corrections performed hourly with an estimated uncertainty of $\sim 2''$. The system temperatures ranged between 40-80 K during the observations.

Position-switching mode was used with a 120 s ON-OFF cadence and a position 1° offset from the target. In total, each of the ten frequency windows were observed between ~ 7.5 and 15 hours on source. Data reduction was performed using the GBTIDL package. The data were placed on the atmosphere-corrected T_A^* scale (Ulich & Haas 1976) and averaged. A polynomial fit was used to remove the baseline. Subsequent smoothing to a spectral resolution of 5.7 kHz ($\sim 0.08 \text{ km s}^{-1}$) improved the signal to noise ratio (SNR) in the weaker features while maintaining at least 3 channels sampling across the narrowest spectral feature observed. This resulted in final RMS noises of 3-5 mK (Table 1)

3. SPECTROSCOPY

For the new species detected here, McCarthy et al. (2000) measured the pure rotational spectra of the isotopologues of several cyanopolynes, including HC₇N, between 6 and 17 GHz, and resolved the nitrogen hyperfine splitting. The rotational spectrum for HC₅¹⁵N was measured by Bizzocchi et al. (2004). The corresponding quantum transitions, frequencies (MHz), line strengths (D²), and upper-level energies (K) for transitions falling within our observational coverage are shown in Table 1.

4. RESULTS AND ANALYSIS

We detected, for the first time, emission from DC₇N and six ¹³C-bearing isotopologues of HC₇N. In addition, we confirm the recent detection of HC₅¹⁵N (Taniguchi & Saito 2017) with the observation of the $J=8\rightarrow7$ transition, which was not reported in that work. For the ¹³C-isotopomers, at least one ΔJ transition between $17\rightarrow16$ and $20\rightarrow19$ was detected for six of the seven isotopomers. In addition, two transitions of DC₅N, two transitions of HC₇N, and a set of 5 hyperfine components of a single ΔJ for HC₅N were also detected. Spectra for these species are shown in Figures 1 and 2. The lines are seen at a $v_{lsr} \sim 5.8$ km s⁻¹, typical of molecules in this source (Kaifu et al. 2004). For the one non-detected isotopomer, H¹³CC₆N, an upper limit on the column density was derived whose value is consistent with the other detected isotopomers.

In TMC-1, the molecular emission can be well described by a single excitation temperature between $T_{ex} \sim 5$ -10 K (Remijan et al. 2006; Loomis et al. 2016). To calculate the column density, we use the formalism described in Hollis et al. (2004) and given by

$$N_T = \frac{Q e^{E_u/T_{ex}}}{\frac{8\pi^3}{3k_B} \nu S_{ij} \mu^2} \times \frac{\frac{1}{2} \sqrt{\frac{\pi}{\ln 2}} \frac{\Delta T_A^* \Delta V}{\eta_B}}{1 - \frac{e^{h\nu/k_B T_{ex}} - 1}{e^{h\nu/k_B T_{bg}} - 1}}. \quad (5)$$

Here N_T is the column density (cm⁻²), Q is the partition function (see below), E_u is the upper state energy of a given transition (K), T_{ex} is the excitation temperature (K), ν is the transition rest frequency (Hz), S_{ij} is the intrinsic line strength, μ^2 is the transition dipole moment squared (J cm³), ΔT_A^* is the peak intensity (K), ΔV is the fitted FWHM linewidth (cm s⁻¹), η_B is the beam efficiency (~ 0.92 at 20 GHz for the GBT), and T_{bg} is the continuum background temperature (2.73 K). Because of the narrow range of upper level energies of the observed transitions, we assume that $T_{ex} = 7$ K for all species.

The total partition function Q accounts for both the rotational and vibrational contributions, as described by

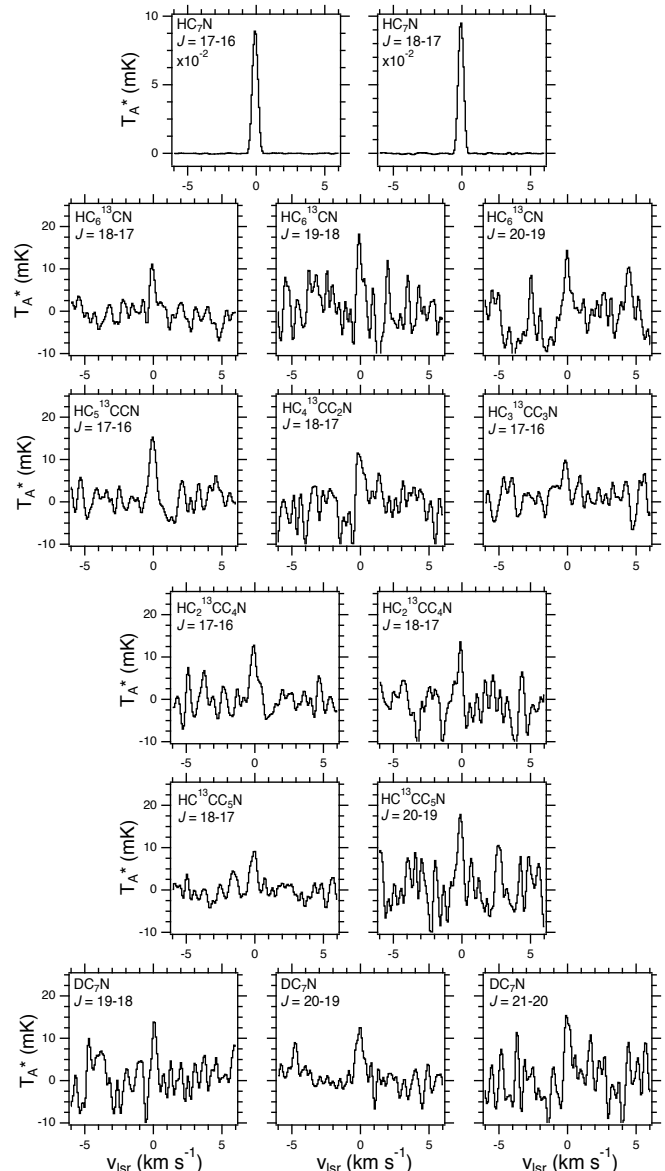


Figure 1. Detected transitions of HC₇N isotopologues, organized by isotope location and corresponding quantum numbers for each transition (labelled on in top left of each spectra). Velocities are given with respect to V_{lsr} of the transition rest frequency, with the listed transition centred at 0 km s⁻¹.

$$Q = Q_{vib} \times Q_{rot}. \quad (6)$$

While the rotational component dominates at interstellar conditions, cyanopolynes can have Q values that can be affected by the vibrational component at even modest excitation temperatures. We utilised the calculated harmonic stretching vibrational wavenumbers (ω) for HC₇N by Botschwina et al. (1997), with the assumption that the partition function will not be significantly

Table 1. Measured and observed frequencies of detected HC₇N and HC₅N isotopomer and isotopologue transitions covered in this work and pertinent line parameters from Gaussian fits.

Species	$J' \rightarrow J''$	Frequency ^a (MHz)	V_{lsr}^b (km s ⁻¹)	ΔT_A^{*c} (mK)	ΔV (km s ⁻¹)	$S_{ij}\mu^2$ (Debye ²)	E_u (K)
HC ₇ N	17→16	19175.959	5.81	909(3)	0.474(2)	394.9	8.283
	18→17	20303.946	5.83	978(2)	0.458(1)	418.2	9.257
HC ₆ ¹³ CN	18→17	20071.326	5.84	12(1)	0.36(5)	418.2	9.151
	19→18	21186.389	5.86	13.2(9)	0.46(3)	441.4	10.168
	20→19	22301.449	5.84	19(3)	0.31(6)	464.7	11.238
HC ₅ ¹³ CCN	17→16	19102.044	5.84	16(1)	0.52(5)	394.9	8.251
HC ₄ ¹³ CC ₂ N	18→17	20294.271	5.89	12(1)	0.54(8)	418.3	9.253
HC ₃ ¹³ CC ₃ N	17→16	19165.136	5.70	9.9(4)	0.50(2)	394.9	8.278
HC ₂ ¹³ CC ₄ N	17→16	19097.498	5.81	12.8(3)	0.48(1)	394.9	8.249
	18→17	20220.870	5.76	14(3)	0.32(8)	418.2	9.219
HC ¹³ CC ₅ N	18→17	20063.864	5.80	9(1)	0.51(7)	418.1	9.148
	20→19	22293.157	5.76	18(3)	0.42(8)	464.6	11.234
H ¹³ CC ₆ N	21→20	23168.899	- ^d	<14.8 ^d	0.4 ^d	487.4	12.231
DC ₇ N	19→18	20721.873	5.97	15(3)	0.34(7)	441.4	9.945
	20→19	21812.486	5.84	12.2(6)	0.62(4)	464.7	10.992
	21→20	22903.097	5.92	16(1)	0.49(6)	487.9	12.091
HC ₅ N	8→7, $F=8\rightarrow8$	21299.750	5.82	32(3)	0.43(4)	0.781	4.600
	8→7, $F=7\rightarrow6$	21301.245				43.3	4.600
	8→7, $F=8\rightarrow7$	21301.261	5.82	2489(11)	0.650(3)	49.2	4.600
	8→7, $F=9\rightarrow8$	21301.272				55.9	4.600
	8→7, $F=7\rightarrow7$	21302.970	5.85	25(2)	0.54(6)	0.781	4.600
HC ₅ ¹⁵ N	8→7	20778.180	5.78	16.9(9)	0.46(3)	150.0	4.487
HC ₄ ¹³ CN	7→6	18454.489	5.80	28(1)	0.76(4)	131.2	3.543
HC ₃ ¹³ CCN	8→7	21281.792	5.82	40(2)	0.59(3)	151.4	4.596
HC ₂ ¹³ CC ₂ N	8→7	21279.200	5.81	42(2)	0.67(4)	150.0	4.596
HC ¹³ CC ₃ N	7→6	18447.612	5.81	20(1)	0.79(5)	130.0	3.541
H ¹³ CC ₄ N	8→7	20746.761	5.81	42(1)	0.59(2)	150.0	4.481
DC ₅ N	8→7	20336.870	5.82	52(2)	0.47(2)	150.001	4.392
	9→8	22878.963	5.86	59(2)	0.54(2)	168.729	5.490

^aMcCarthy et al. (2000) had a 1 σ experimental uncertainty of \sim 2 kHz.

Bizzocchi et al. (2004) had a 1 σ experimental uncertainty of \sim 15 kHz.

^b1 σ uncertainties from Gaussian fits are \sim 0.5 kHz (0.08 km s⁻¹). Given the SNR of the detected lines (\sim 3-5) and the linewidth, we estimate the uncertainty in the observed line centres to be \sim 3.7 kHz.

^c1 σ uncertainty of the Gaussian fit to each line given.

^dUpper limit of line peak set by 3 \times RMS at transition frequency.

For purposes of N_T calculations, ΔV was estimated to be 0.4 km s⁻¹.

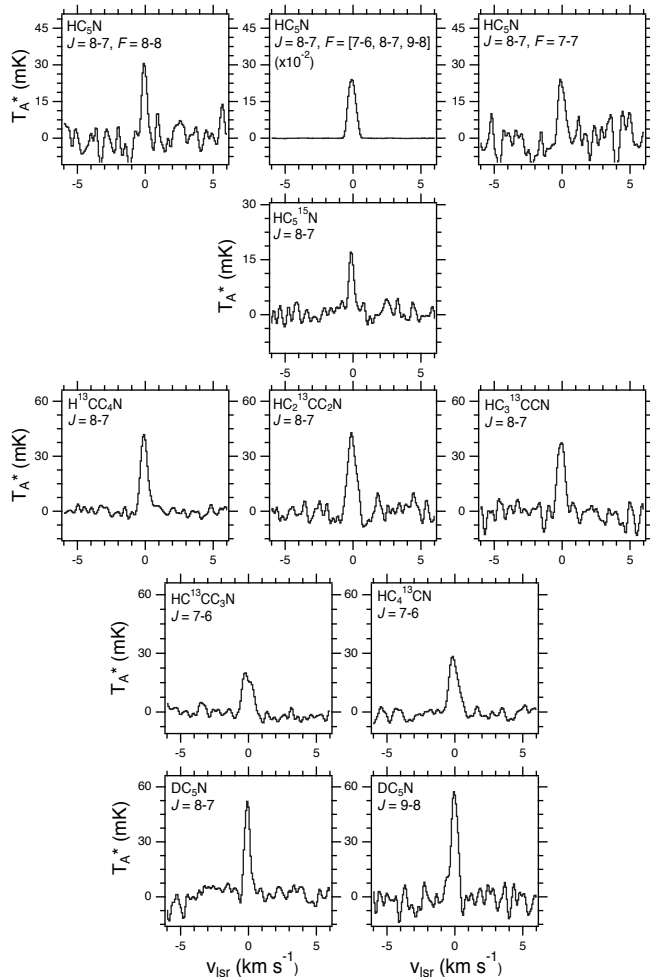


Figure 2. Detected transitions of HC_5N isotopologues, organized by isotope-location and corresponding quantum numbers for each transition (labelled on in top left of each spectra). Velocities are given with respect to V_{lsr} of the transition rest frequency, with the listed transition centred at 0 km s^{-1} .

impacted by the presence or location of ^{13}C or D in the molecule. The lowest three energy levels for HC_7N are 62 , 163 , and 280 cm^{-1} (92 , 241 , and 415 K , respectively). At 7 K , the change from the vibrational contribution is negligible ($\Delta Q/Q [7 \text{ K}] \sim 10^{-6}$); this correction becomes $\gtrsim 1\%$ at $T_{\text{ex}} \gtrsim 20 \text{ K}$. Similar behavior is seen for HC_5N isotopologues.

Values of ΔT_A^* and ΔV were determined by Gaussian fits to the lines (see Table 1). For species with more than one transition, a single column density was obtained based on a least-squares fit to reproduce the integrated line intensities, with a weighting based on the SNR of the lines. The calculated column densities are summarized in Table 2.

To calculate the uncertainties, we considered both the measurements and analysis. The absolute flux calibration procedure for the GBT is estimated to have $\sim 20\%$ uncertainty. We include 1σ uncertainties in ΔT_A^* and ΔV derived from the Gaussian fits. Due to our assumption of a single excitation temperature of $T_{\text{ex}} = 7 \text{ K}$, we find that variations of previously calculated excitation temperatures ($5\text{--}10 \text{ K}$) result in between $15\text{--}20\%$ uncertainty in the resulting column densities for HC_7N isotopologues and $\sim 5\%$ for HC_5N isotopologues. We assume that the source is significantly extended beyond the GBT beam, and thus the contributions to the uncertainty from pointing are trivial, and no beam filling correction is applied. The resulting column densities, with all uncertainties added in quadrature, are given in Table 2.

For the purposes of calculating the molecular abundances, we used the H_2 column density derived by Gratier et al. (2016) from observations from Kaifu et al. (2004) of $N_{\text{H}_2} = 10^{22} \text{ cm}^{-2}$, with the caveat that the beam size of the survey performed with the Nobeyama 45m dish telescope is about twice that of the GBT, and thus a non-isotropic distribution of H_2 , or any molecular species, may result in different column densities derived between the observations. These abundances are also given in Table 2. In addition to comparing the relative column densities of the isotopomers, an average value across all detected ^{13}C -isotopomers is also calculated. The column density for each detected species was averaged, weighted by the error of each value, and are also tabulated in Table 2. These calculated values are compared to previous observations in Table 3.

4.1. Treatment of Hyperfine Splitting

For HC_5N , the brightest detected signal is a blend of three hyperfine components. Two additional, weaker $\Delta F=0$ hyperfine components are resolved. The central, bright feature has been shown to be slightly optically thick (Gratier et al. 2016). Our calculation of the column density was therefore derived using the two, optically-thin hyperfine components, yielding a value of $5(1) \times 10^{13} \text{ cm}^{-2}$, in agreement with the previous work (MacLeod et al. 1981; Gratier et al. 2016; Taniguchi et al. 2016a).

For all other species studied here, the hyperfine components are unresolved. As such, for the purposes of calculating column densities, the hyperfine splitting is not considered and the integrated intensity is used instead. This likely slightly overestimates the linewidths due to the blending of hyperfine components. However, this is still a reasonable assumption, as the lines are well-modeled by a single Gaussian lineshape, and thus

Table 2. Measured column densities and upper limits for isotopomers and isotopologues discussed here, and, when relevant, the isotopic ratio (i.e. $^{12}\text{C}/^{13}\text{C}$; H/D; $^{14}\text{N}/^{15}\text{N}$).

Species	N_T ($\times 10^{11} \text{ cm}^{-2}$)	N_T/N_{H_2} ($\times 10^{-11}$)	Isotopic Ratio [†]	\mathcal{R}^\ddagger
HC ₇ N	139(36)	139(36)	-	-
HC ₆ ¹³ CN	1.7(6)	1.7(6)	83(34)	85(35)
HC ₅ ¹³ CCN	2.6(7)	2.6(7)	52(20)	53(20)
HC ₄ ¹³ CC ₂ N	2.1(7)	2.1(7)	66(27)	67(28)
HC ₃ ¹³ CC ₃ N	1.6(4)	1.6(4)	88(32)	90(33)
HC ₂ ¹³ CC ₄ N	1.8(5)	1.8(5)	78(31)	79(32)
HC ¹³ CC ₅ N	2.0(7)	2.0(7)	71(31)	73(31)
H ¹³ CC ₆ N	<2.2	<2.2	>63	>64
DC ₇ N	2.5(9)	2.5(9)	56(24)	61(29)
Weighted ¹³ C Average Value	1.9(2)	1.9(2)	73(21)	75(21)
Total ¹³ C-isotopologue*	13.3(1.8)	13.3(1.8)	9.6(2.7)% [⊖]	9.4(2.7)% [⊖]
HC ₅ N	492(122)	492(122)	-	-
HC ₅ ¹⁵ N	1.5(4)	1.5(4)	326(109)	344(114)
HC ₄ ¹³ CN	4.6(9)	4.6(9)	107(35)	108(36)
HC ₃ ¹³ CCN	4.4(9)	4.4(9)	111(37)	113(38)
HC ₂ ¹³ CC ₂ N	5.3(1.2)	5.3(1.2)	93(31)	94(32)
HC ¹³ CC ₃ N	3.4(7)	3.4(7)	144(47)	146(49)
H ¹³ CC ₄ N	4.8(1.0)	4.8(1.0)	102(33)	103(34)
DC ₅ N	5.3(1.2)	5.3(1.2)	92(30)	96(32)
Weighted ¹³ C Average Value	4.4(4)	4.4(4)	111(30)	113(31)
Total ¹³ C-isotopologue*	22(3)	22(3)	4.5(1.2)% [⊖]	4.4(1.2)% [⊖]

[†] Column density ratio of most common isotopologue vs less common species given (e.g. $^{12}\text{C}/^{13}\text{C}$; H/D; $^{14}\text{N}/^{15}\text{N}$)

[‡] Isotope ratio, including the all other singly-substituted isotopologues (see section 4.2)

* Calculated by 7 times the weighted average of ¹³C values

⊖ Percent of total molecular density of HC_nN containing a single ¹³C substitution

will not significantly impact the resulting column densities, which are calculated via the integrated intensity in Equation 5.

4.2. Calculation of Line Ratios and Total Values

Relative isotopic ratios calculated for H/D, $^{12}\text{C}/^{13}\text{C}$, and $^{14}\text{N}/^{15}\text{N}$ are tabulated in Table 2. It should be noted that none of the uncertainties described above for determining the column densities should cancel out in the calculation of the ratios, as the uncertainty in the absolute flux calibration comes from the time and frequency variability of the calibrator source. For HC₇N, where we lack a detection of H¹³CC₆N, we calculate a

total column density of all ¹³C-substituted isotopomers by scaling the average column density for the isotopologue by the number of isotopomers, which is equal to the number of carbon atoms in the molecule..

As discussed in Langston & Turner (2007), the presence of isotopologues affects the observed abundances of the main isotopic species, especially for increasingly complex molecules. As the number of atoms in a species increases, so does the probability that any given molecule will contain at least a single isotope-substituted atom. This would be most apparent in fullerenes like C₆₀, where a Galactic $^{12}\text{C}/^{13}\text{C}$ ratio

of ~ 68 , or 1.5%, (Milam et al. 2005) would result in $\sim 60\%$ of all C_{60} containing, at least one ^{13}C substitution. Similarly, it may be important to consider the size of the molecule when comparing the total isotopologue fraction. Given the same ISM ratio and purely ^{13}C -substitution, and no additional chemical bias, the larger cyanopolyynes would be expected to have the following total singly-substituted ^{13}C fractional abundances: HC_5N (7.2%), HC_7N (10%), HC_9N (12%), $HC_{11}N$ (15%).

Given the non-trivial fraction of isotopologues for a given large species, as the observational capabilities improve it will likely be important to consider their abundances when calculating isotopic ratios. For the purposes of comparing to standard ISM values, a more accurate ratio for fractionation would be (taking ^{15}N of HC_5N as an example)

$$\mathcal{R} = \frac{N_T(HC_5N) + \sum N_T(H^{13}CC_4N \text{ isotopomers}) + N_T(DC_5N)}{N_T(HC_5^{15}N)}. \quad (7)$$

Here, it is assumed that doubly-substituted isotopologues do not contribute significantly yet to the ratio, which may not be valid for species as large as C_{60} . In addition to the standard column density ratio given, this additional value is also given in Table 2, even though the relative differences ($\sim 10\%$) are still well within the observational uncertainties. As chemical models increase their molecular complexity, it will become increasingly important to consider the isotopologues of large molecules, as well as their precursor species. This is already shown by (Majumdar et al. 2017) on the modeling of deuterated species toward TMC-1, where the robust inclusion of deuterated chemistry was found to alter the chemical time-scales by up to a factor of 3. This effect will also be more apparent when species contain at least one atom with a higher natural percentage in non-standard isotopes, such as S and Cl and species common in silicate grain precursors (Mg, Si, Ti, Fe). While the upper limit of this effect will likely decrease the modeled abundances by no more than roughly factor of 2, it is certainly an important effect to consider in the future.

5. DISCUSSION

Constraining the chemistry for larger cyanopolyynes requires the consideration of both the possible formation routes, as described in §1, and the many precursor species, whose isotopic ratios across the literature are summarized in Table 3. The analysed isotopic ratios in this work agree reasonably well with previous observations or lower limits for the same species. The general spread in values for a given species may be attributable to the spread in excitation temperatures used (5-10 K) or inconsistent treatments of both the optical depths

and hyperfine structure in the column density calculations for HC_5N and HC_7N . For HC_3N , the relative enhancement of $^{12}C/^{13}C$ for $HC_2^{13}CN$ and the agreement of the $^{14}N/^{15}N$ ratio with Galactic measurements of CN both indicate that this species may be efficiently produced through the reaction containing CN, as described in Mechanism 1 (Takano et al. 1998). Taniguchi et al. (2016a) showed that HC_5N does not show this same trend. Through the comparison of the various isotopologues studied here, it is further possible to differentiate among the three mechanisms described in §1 for both HC_5N and HC_7N .

In contrast to the $\sim 40\%$ enhancement of $HC_2^{13}CN$ over $HC^{13}CCN$ and $H^{13}CC_2N$ (Takano et al. 1998), the relative isotopic ratios of all ^{13}C isotopomers for both HC_7N and HC_5N were all consistent with their respective average values within our uncertainties. The ratio of column densities of the $HC_{n-1}^{13}CN$ isotopomers to the weighted average ^{13}C -isotopologue values can be used to more explicitly test the significance of Mechanism 1 in the formation of larger cyanopolyynes. Specifically the column densities of $HC_4^{13}CN$ and $HC_6^{13}CN$ agree with their respective ^{13}C average values to $<10\%$. Because both HC_5N and HC_7N do not display the $HC_{n-1}^{13}CN$ enhancement, this provides evidence that larger cyanopolyynes are not produced from CN to the same extent as HC_3N . Even though $H^{13}CC_6N$ was not detected here, the formation route from CN should not significantly alter the $^{12}C/^{13}C$ isotopic ratio of this molecule and so does not conflict with this conclusion. Thus, we can eliminate Mechanism 1 as the dominant pathway for both HC_5N and HC_7N .

As seen Table 3, while still in agreement within the uncertainties, all isotopologues of HC_5N are found to be depleted (i.e. larger isotopic ratios) relative to HC_3N and HC_7N , showing that this isotopic depletion seen in Taniguchi et al. (2016a) does not continue for HC_7N . While the average $^{12}C/^{13}C$ ratio for HC_7N agrees very well with ratios corresponding to HCN, Galactic measurements of CN, and the two non-enhanced isotopomers of HC_3N , the average HC_5N $^{12}C/^{13}C$ ratio is $\sim 50\%$ larger than any of these values. For $HC^{15}N$, the $^{14}N/^{15}N$ ratio is much larger compared to HC_3N and Galactic measurements of CN, which have been shown to have enhanced ^{15}N isotopologue abundances relative to average ISM values (Roueff et al. 2015; Ritchey et al. 2015; Hily-Blant et al. 2013). Similarly, the DC_5N abundance is diminished by roughly the same percentage relative to HC_7N as the ^{13}C -substituted isotopologues in our data. However, large uncertainties due to the SNR of our data and inconsistent treatment of the excitation temperature and hyperfine splitting across the literature

Table 3. Comparison of observed ratios to previous values of cyanopolynes and related species in the literature.

Ratio	$^{12}\text{C}/^{13}\text{C}$						H/D					$^{14}\text{N}/^{15}\text{N}$				
	Source	HC ₇ N	HC ₅ N	HC ₃ N	HCN	CN [†]	ISM [‡]	HC ₇ N	HC ₅ N	HC ₃ N	HCN	HC ₅ N	HC ₃ N	HCN	CN [†]	ISM [‡]
This work	73(21)	111(30)	-	-	-	-	-	56(24)	92(30)	-	-	326(109)	-	-	-	-
A	87 ⁺³⁵ ₋₁₉	-	-	-	-	-	-	>59	-	-	-	>52	-	-	-	-
B	-	54 ⁺²¹ ₋₂₂	130 ⁺²³ ₋₅₀	-	-	-	-	-	52 ⁺²⁶ ₋₂₀	81 ⁺⁸² ₋₆₈	-	-	-	-	-	-
C	-	94(6)	-	-	-	-	-	-	-	-	-	-	-	-	-	-
D	-	-	77(7) [*]	-	-	-	-	-	-	-	-	-	-	-	-	-
	-	-	55(7) [*]	-	-	-	-	-	-	-	-	-	-	-	-	-
E	-	-	56.8 [⊖]	69 [⊖]	-	-	-	-	-	71 [⊖]	91(38)	-	-	-	-	-
F	-	-	-	-	68(15)	-	-	-	-	-	-	-	-	-	-	-
G	-	-	-	-	-	88.9(6)	-	-	-	-	-	-	-	-	-	424(3)
H	-	-	-	-	-	-	-	-	83 ⁸³ ₋₂₁	-	-	-	-	-	-	-
I	-	-	-	-	-	-	-	-	62(12)	>17(6)	-	-	-	-	-	-
J	-	-	-	-	-	-	-	-	-	22(12)	-	-	-	-	-	-
K	-	-	-	-	-	-	-	-	-	-	344(53)	257(54)	-	-	-	-
L	-	-	-	-	-	-	-	-	-	-	-	-	323(63) ^{‡*}	-	-	-
M	-	-	-	-	-	-	-	-	-	-	-	-	-	274(18)	-	-
N	-	-	-	-	-	-	-	-	-	-	-	-	-	-	-	441(5)

[†] CN values acquired from observations of Galactic diffuse molecular clouds

[‡] ISM values acquired from solar system measurements (i.e. Local ISM)

^{*} First value is average of H¹³CC₂N and HC¹³CCN. Second value is for HC₂¹³CN

[⊖] Uncertainties not given for most values in Turner (2001)

^{‡*} Value given in literature is H¹³CN/HC¹⁵N, which we scaled by the HCN/H¹³CN ratio from Turner (2001)

References: [A] Langston & Turner (2007); [B] Gratier et al. (2016); [C] Taniguchi et al. (2016a); [D] Takano et al. (1998); [E] Turner (2001);

[F] Milam et al. (2005); [G] Meibom et al. (2007); [H] MacLeod et al. (1981); [I] Schloerb et al. (1981); [J] Howe et al. (1994);

[K] Taniguchi & Saito (2017); [L] Ikeda et al. (2002); [M] Ritchey et al. (2015); [N] Marty et al. (2011)

results in a large spread of H/D for any given species, making this trend less certain than for the $^{12}\text{C}/^{13}\text{C}$ and $^{14}\text{N}/^{15}\text{N}$ ratios. Considering all of this, the mixture of formation and destruction methods for cyanopolynes appears to not be consistent across the molecular family.

More specifically, because the $^{12}\text{C}/^{13}\text{C}$ ratio in HC₅N is not in agreement with the ratios observed for HC₃N and HC₇N, the carbon fractionation in these species does not appear to be inherited from the next-smallest cyanopolyne, as would be predicted by Mechanism 2. Given that Mechanism 2 is inefficient for HC₅N and HC₇N production, the only remaining formation pathway proposed is the reaction of hydrocarbon ions with nitrogen atoms (Mechanism 3), and thus is the best prediction for the dominant production route for large cyanopolynes. If the trends discussed here are found to be true, a dedicated investigation of the underlying chemistry of hydrocarbon ions and undetected C_nH isotopologues may reveal a unique ^{13}C distribution and provide constraints on the formation of cyanopolynes and other carbon-chain molecules.

6. CONCLUSIONS

The interstellar detections of DC₇N, six of the seven ^{13}C -bearing isotopologues of HC₇N, and HC₅¹⁵N are reported toward TMC-1 with observations using the GBT. Column densities for each of the detected species and an upper limit for H¹³CC₆N, were calculated, as well as the resulting isotopic ratios for each species. From analysis of these ratios, we find that:

- There are no significant $^{12}\text{C}/^{13}\text{C}$ variations among the isotopomers of both HC₅N and HC₇N, implying that CN is not an important precursor for their formation.
- For all isotopologues studied in this work, while the values still agree within our uncertainties, HC₅N is found to be isotopically depleted relative to other HC_nN molecules and this trend does not continue onto HC₇N. Given also that the ^{13}C and ^{15}N ratios for HC₃N and HC₇N agree very well, there is evidence that cyanopolynes are not efficiently formed from their next-smallest molecular family member, HC_{n-2}N
- As a result, the only remaining significant formation route for HC₅N and HC₇N is the reaction of hydrocarbon ions and nitrogen atoms

ACKNOWLEDGEMENTS

A.M.B. is a Grote Reber Fellow, and support for this work was provided by the NSF through the Grote Reber Fellowship Program administered by Associated Universities, Inc./National Radio Astronomy Observatory and the Virginia Space Grant Consortium. E. H. thanks the National Science Foundation for support of his astrochemistry program. S.V.K. acknowledges support from Basic Research Program P-7 of the Presidium of the Russian Academy of Sciences. A.M.B. thanks C.N. Shingledecker for helpful discussions on chemical models for cyanopolynes. B.A.M. thanks K. L. Lee for helpful discussions regarding vibrational energy levels. The

National Radio Astronomy Observatory is a facility of the National Science Foundation operated under cooperative agreement by Associated Universities, Inc. The Green Bank Observatory is a facility of the National Sci-

ence Foundation operated under cooperative agreement by Associated Universities, Inc. The authors thank the anonymous referee for comments that improved the quality of this manuscript.

REFERENCES

- Araki M., Takano S., Sakai N., et al., 2016, *ApJ*, **833**, 291
- Bell M. B., Avery L. W., MacLeod J. M., et al., 1992, *ApJ*, **400**, 551
- Bell M. B., Feldman P. A., Travers M. J., et al., 1997, *ApJL*, **483**, L61
- Benson P. J. & Myers P. C., 1989, *ApJS*, **71**, 89
- Bizzocchi L., Degli Esposti C., & Botschwina P., 2004, *Journal of Molecular Spectroscopy*, **225**, 145
- Botschwina P., Horn M., Markey K., et al., 1997, *Molecular Physics*, **92**, 381
- Broten N. W., Oka T., Avery L. W., et al., 1978, *ApJL*, **223**, L105
- Bujarrabal V., Guelin M., Morris M., et al., 1981, *A&A*, **99**, 239
- Cernicharo J., Heras A. M., Tielens A. G. G. M., et al., 2001, *ApJL*, **546**, L123
- Fukuzawa K., Osamura Y., & Schaefer III H. F., 1998, *ApJ*, **505**, 278
- Gratier P., Majumdar L., Ohishi M., et al., 2016, *ApJS*, **225**, 25
- Guzman-Ramirez L., Zijlstra A. A., Níchuimín R., et al., 2011, *MNRAS*, **414**, 1667
- Hasegawa T. I., Herbst E., & Leung C. M., 1992, *ApJS*, **82**, 167
- Herbst E., 1983, *ApJS*, **53**, 41
- Herbst E. & Leung C. M., 1990, *A&A*, **233**, 177
- Herbst E. & Millar T. J., 2008, *The Chemistry of Cold Interstellar Cloud Cores in Low Temperatures and Cold Molecules*. World Scientific
- Herbst E., Adams N. G., & Smith D., 1984, *ApJ*, **285**, 618
- Hily-Blant P., Bonal L., Faure A., et al., 2013, *Icarus*, **223**, 582
- Hollis J. M., Jewell P. R., Lovas F. J., et al., 2004, *ApJ*, **613**, L45
- Howe D. A., Millar T. J., Schilke P., et al., 1994, *MNRAS*, **267**, 59
- Huntress Jr. W. T., 1977, *ApJS*, **33**, 495
- Ikeda M., Hirota T., & Yamamoto S., 2002, *ApJ*, **575**, 250
- Irvine W. M., Hoglund B., Friberg P., et al., 1981, *ApJL*, **248**, L113
- Kaifu, N., Ohishi, M., Kawaguchi, K., et al., 2004, *PASJ*, **56**, 69
- Kirkpatrick, A., Alberts, S., Pope, A., et al., 2017, *PASJ*, **849**, 111
- Knight J. S., Freeman C. G., McEwan M. J., et al., 1986, *MNRAS*, **219**, 89
- Langston G. & Turner B., 2007, *ApJ*, **658**, 455
- Loomis, R. A., Shingledecker, C. N., Langston, G., et al., 2016, *MNRAS*, **463**, 4175
- MacLeod J. M., Avery L. W., & Broten N. W., 1981, *ApJL*, **251**, L33
- Majumdar, L., Gratier, P., Ruaud, M., et al., 2017, *MNRAS*, **466**, 4470
- Marty B., Chaussidon M., Wiens R. C., et al., 2011, *Science*, **332**, 1533
- Mauersberger R., Henkel C., & Sage L. J., 1990, *A&A*, **236**, 63
- McCarthy M. C., Travers M. J., Kovács A., et al., 1997, *ApJS*, **113**, 105
- McCarthy M. C., Levine E. S., Apponi A. J., et al., 2000, *JMoSp*, **203**, 75
- McCarthy M. C., Gottlieb C. A., Gupta H., et al., 2006, *ApJL*, **652**, L141
- McGuire B. A., Burkhardt A. M., Shingledecker C. N., et al., 2017, *ApJL*, **843**, L28
- Meibom A., Krot A. N., Robert F., et al., 2007, *ApJL*, **656**, L33
- Milam S. N., Savage C., Brewster M. A., et al., 2005, *ApJ*, **634**, 1126
- Ohishi M. & Kaifu N., 1998, *Faraday Discuss.*, **109**, 205
- Remijan A. J., Wyrowski F., Friedel D. N., et al., 2005, *ApJ*, **626**, 233
- Remijan A. J., Hollis J. M., Snyder L. E., et al., 2006, *ApJL*, **643**, L37
- Ritchey A. M., Federman S. R., & Lambert D. L., 2015, *ApJL*, **804**, L3
- Roueff E., Loison J. C., & Hickson K. M., 2015, *A&A*, **576**, A99
- Ruaud M., Wakelam V., & Hersant F., 2016, *MNRAS*, **459**, 3756
- Schiff H. I. & Bohme D. K., 1979, *ApJ*, **232**, 740
- Schloerb F. P., Snell R. L., Langer W. D., et al., 1981, *ApJL*, **251**, L37
- Snyder L. E., Hollis J. M., Jewell P. R., et al., 2006, *ApJ*, **647**, 412

Takano, S., Masuda, A., Hirahara, Y., et al., 1998, *A&A*,
329, 1156
Taniguchi K. & Saito M., 2017, *PASJ*, 69, L7
Taniguchi K., Ozeki H., Saito M., et al., 2016a, *ApJ*, 817,
147
Taniguchi K., Saito M., & Ozeki H., 2016b, *ApJ*, 830, 106

Taniguchi K., Ozeki H., & Saito M., 2017, *ApJ*, 846, 46
Turner B. E., 2001, *ApJS*, 136, 579
Ulich B. L. & Haas R. W., 1976, *ApJS*, 30, 247
Watson W. D., Anicich V. G., & Huntress Jr. W. T., 1976,
ApJL, 205, L165
Winnewisser G. & Walmsley C. M., 1979, *Ap&SS*, 65, 83